The dynamics and pH-dependence of Ag43 adhesins' self-association probed by atomic force spectroscopy

Adrien Jacquot, Chizuko Sakamoto, Angelina Razafitianamarahavo, Céline Caillet, Jenny Merlin, Ahmad Fahs, Jean-Marc Ghigo, Jérôme F. L. Duval, Christophe Beloin, Grégory Francius

Dynamics and pH-dependence of Ag43 adhesins self-association probed by Atomic Force Spectroscopy

A. Jacquot,[1,2] C. Sakamoto,[3,4] A. Razafitianamaharavo,[5,6] C. Caillet,[5,6] J. Merlin,[5,6] A. Fahs,[1,2] J.M. Ghigo,[3] J.F.L. Duval[5,6], C. Beloin[3] and G. Francius[1,2*]

[1] Université de Lorraine, Laboratoire de Chimie Physique et Microbiologie pour l'Environnement, UMR 7564, Villers-lès-Nancy, F-54601, France.

[2] CNRS, Laboratoire de Chimie Physique et Microbiologie pour l'Environnement, UMR 7564, Villers-lès-Nancy, F-54601, France.

[3] Institut Pasteur, Unité de Génétique des Biofilms, 25-28 rue du Dr Roux, Paris cedex 15, F-75724, France.

[4] Université Paris Diderot, Sorbonne Paris Cité, Cellule Pasteur, rue du Dr Roux, Paris, F-75015, France.

[5] Université de Lorraine, Laboratoire Interdisciplinaire des Environnements Continentaux, UMR 7360, Vandœuvre-lès-Nancy, F-54501, France.

[6] CNRS, Laboratoire Interdisciplinaire des Environnements Continentaux, UMR 7360, Vandœuvre-lès-Nancy, F-54501, France.

* Corresponding author:

Email: gregory.francius@univ-lorraine.fr

Phone: (33) 03 83 68 52 36

Abstract

Self-associating auto-transporter (SAAT) adhesins are two-domains cell surface proteins involved in bacteria auto-aggregation and biofilm formation. Antigen 43 (Ag43) is a SAAT adhesin commonly found in *Escherichia coli* whose variant Ag43a has been shown to promote persistence of uropathogenic *E. coli* within the bladder. The recent resolution of the tri-dimensional structure of the 499 amino-acids α-domain in Ag43a has shed light on the possible mechanism governing the self-recognition of SAATs adhesins, in particular the importance of *trans*-interactions between the L shape β-helical scaffold of two α-domains of neighboring adhesins. In this study, we use Single-Molecule Force Spectroscopy (SMFS) and Dynamic Force Spectroscopy (DFS) to unravel the dynamics of Ag43-self association under various pH and molecular elongation rates conditions that mimic the situations encountered by *E. coli* in its natural environment. Results evidenced an important stretchability of Ag43α with unfolding of sub-domains leading to molecular extension as long as 150 nm. Nanomechanical analysis of molecular stretching data suggested that self-association of Ag43 can lead to the formation of dimers and tetramers driven by rapid and weak *cis*- as well as slow but strong *trans*-interaction forces with magnitude as large as 100-250 pN. The dynamics of *cis*- and *trans*- interactions were demonstrated to be strongly influenced by pH and applied shear force, thus suggesting that environmental conditions can modulate Ag43-mediated aggregation of bacteria at the molecular level.

Keywords:

Bacterial adhesins, Antigen 43, unwinding, molecular sliding, AFM

Introduction

Bacterial adhesion onto abiotic surfaces and host tissues, as well as bacteria-bacteria interactions are key processes for colonization, biofilm formation and further infection. These different interactions are commonly mediated by surface appendages exposed at the bacterial cell surface.[1, 2] Large heteropolymeric appendages such as fimbriae are generally used by the bacteria to interact with surfaces over large separation distances, while shorter adhesins such as self-associating autotransporters (SAATs) adhesins transported by type V secretion are capable of promoting intimate interactions between bacteria.[3, 4] Prototypical members of this family of SAAT adhesins are AidA, an adhesin originally characterized in an *E. coli* O126:H27 strain isolated from a pediatric patient with diarrhea,[5] TibA, first found in the ETEC O78:H11 strain H10407,[6] and the Antigen 43 adhesin (Ag43), one of the most abundant outer membrane proteins in *E. coli*.[7, 8] Like other AidA-I-type adhesin autotransporters, *E. coli* Antigen 43 is a short and rigid, monomeric adhesin composed of a C-terminal integral outer membrane β domain through which is exported a N-terminal passenger α domain (Ag43α).[9, 10] After its autocatalytic cleavage, Ag43α (499 aa) remains loosely anchored to Ag43 β domain and forms a β-strand helix that protrudes 10 nm from the cell surface.[11-14] Like other AidA-I-type adhesin autotransporters, this adhesin is able to promote cell-cell interactions, and subsequent bacterial autoaggregation [11, 15] and biofilm formation [3, 16-18] through homomeric recognition of its α-domain potentially folded as a β helix. Some Ag43 variants have been further shown to facilitate the persistence of uropathogenic *E. coli* within the bladder,[19, 20] to promote uptake of- and resistance to- antimicrobial agents and protection of *E. coli* against polymorphonuclear neutrophils.[11, 21]

In 2011, the structure of the α-domain of the AT Hap protein from *Haemophilus influenzae* was resolved, which opened a route for elucidating the relationship between structure and homophilic interaction mechanisms of the SAATs.[22] In the Hap protein, homophilic

recognition is promoted by the interaction in *trans* configuration of the α-domain along a 7-turn right-handed β-helix, with ~19 residues in each turn. More recently, Heras *et al*. resolved the crystallographic structure of the Ag43a variant α-domain of uropathogenic *E. coli* strain CFT073.[14] As previously predicted,[11] they demonstrated that the functional 499 amino-acids α-domain of this SAAT protein is a 3 stranded β-helix structure comprising 23 complete turns with an average of 20 amino-acids per turn, each turn being composed of three faces marked by the arrows depicted in **Figure S2**, thus forming a triangular structure. Interestingly, Ag43aα displays a twisted L-shaped β-helical structure that plays a major role in the self-association and cell aggregation *via* a molecular "Velcro-type" mechanism where the dimerization of the α-domain is ensured by multiple hydrogen bonds between the two twisted beta-helical structure coil around each other in a *trans*/head-to-tail configuration.[14] A modeling of the α-domain of *E. coli* K-12 Ag43 that share 81.7% identity with that of UPEC CFT073 Ag43a, revealed that this domain also probably displays a twisted L-shaped β-helical structure (**Figure S2**). However, little is known on the self-association of beta-helical proteins, in particular its dynamics, its dependence on medium composition including pH, and the way it is connected to the intrinsic mechanical and structural properties of the interacting proteins domains. These key issues remain difficult to address at the nanoscale from crystallography or X-ray scattering techniques (SAXS, WAXS) and macroscopic observations of self-aggregation of bacterial cells are useless in this perspective too.

Since the last decade, derivative techniques of atomic force microscopy (AFM) were developed for probing the physico-chemical properties of biomolecules.[23-26] Techniques such as Dynamic Force Spectroscopy (DFS) and Single-Molecule Force Spectroscopy (SMFS) now allow access to molecular dynamic processes, chemical or surface reactivity, conformational properties, and interactions between single molecules.[27, 28] For the sake of example, Single-Molecule Force Spectroscopy (SMFS) was recently used to unravel and

explain the binding mechanism of BCAM0224 auto-transporter adhesins involved in respiratory infections and secreted by *Burkholderia cenocepacia*.[29] The authors evidenced that the BCAM0224 adhesin behaves like a nanospring when subjected to external shear forces and can form both homomeric and heteromeric interactions that enhance adhesion to immune cells with corresponding forces as large as 120 pN. [29] Using a similar technique, the nanomechanical properties of LapA adhesin expressed by *Pseudomonas fluorescens*, or type 1 fimbriae attached to mannose were investigated under various pH, ionic strength and shear force conditions.[30, 31]

In this work, we report a systematic investigation of the impact of solution pH and externally applied shear force on the dynamics of *E. coli* K-12 Ag43 α-domain (Ag43α) unfolding and molecular self-association. The conditions tested in this work mimic those met by *E. coli* cells in their natural environment. Our experiments are carried out using functionalized AFM probes specific to Ag43α interacting with either model surfaces functionalized by Ag43 adhesins or with Ag43-decorated *E. coli* K-12 cells. Retraction force curves were recorded at different pH values ranging from 3 to 9 and were analyzed on the basis of the Worm Like Chain (WLC) model in order to quantify the impact of pH on the conformation properties of Ag43 structure. Dynamic force spectroscopy (DFS) measurements were further performed to investigate the dynamics of Ag43 self-association and unfolding under a wide range of pH and pulling rate conditions. Results obtained from DFS and SMFS experiments were finally supported by macroscopic bacterial auto-aggregation assays. We show that self-association forces between Ag43 α-domains are mainly driven by *trans* interactions of α-domains as strong as 100-250 pN, and we suggest the further contributions of possible *cis* interactions between these domains at sufficiently large values of pH and elongation rate. In addition, the existence of a tetrameric structure composed of Ag43 dimers is hypothesized from inspection of molecular stretching data collected by AFM. Such structure results from the coexistence of

trans- and *cis*- interactions, and its existence is mediated by the lifetime of these interactions and by the solution pH conditions. Our results bring novel information on the mechanical properties of β-helical proteins and on the dynamics of their homomeric interactions.

Results

AFM nanogold-mediated analysis of cells expressing or not Ag43 adhesins.

The surface properties (morphology and adhesion) of *E. coli* K-12 cells constitutively producing or not Ag43 (E2498 and E2152, respectively) were investigated by AFM in PeakForce Mapping ™ mode using a functionalized His-Ag43α coated tip where the histidine tag was fused at the N-terminal part of Ag43 α-domain. The obtained adhesion maps collected with the functionalized AFM-tip (**Figure S1**) revealed that the only E2498 strain exhibited a moderately adhesive bacterial cell wall surface. These results confirmed the presence of Ag43 adhesins over the cell wall of the E2498 strain and they further highlight the specific self-recognition of Ag43 located at the bacterial surface and on the AFM tip. To further localize the Ag43 adhesins by virtue of Ag43α-Ag43α homomeric interactions, we imaged bacterial cells constitutively producing Ag43 or not after incubation with nanogold particles grafted with His-Ag43α where the histidine tag is fused at the N-terminal part of Ag43 α-domain. When experiments were performed with cells E2498 constitutively expressing Ag43, we observed the presence of spherical structures 20 to 200 nm in diameter over and around the bacterial cells (**Figure 1a**, white arrows). NTA-nanogold particles are 5 nm in diameter before functionalization and the estimated size of Ag43α domain is 10 nm. Large structures (> 20 nm) are then supposedly composed of 10-25 nm diameter substructures interacting following homomeric recognition of Ag43α. These large structures did not

correspond to aggregated nanogold particles and their observation depended on the presence of Ag43 on the *E. coli* cell surface since they were not detected for the strain E2152 deleted for the *agn43* gene (**Figure 1b**). These results support that the presence of the aforementioned structures results from homomeric interactions taking place between Ag43α carried by nanogold and Ag43α located at the *E. coli* cell surface. The presence of structures with characteristic dimensions of *ca* 200 nm suggested that more than two molecules of Ag43α may interact in order to form such large complexes.

Analysis of Ag43α self-association by dynamic force spectroscopy

The dynamics of the adhesin conformational structure during self-recognition process is an important issue to address for understanding the auto-aggregation mechanism and the nature of the underlying protein-protein interactions. Single Molecule Force Spectroscopy (SMFS) and Dynamic Force Spectroscopy (DFS) are very relevant tools in that respect because they enable the analysis of the protein conformational changes and dynamics thereof during protein-protein interactions on living cell surfaces.[28, 36] Therefore, combined SMFS and DFS experiments were performed here in order to (i) evaluate the interaction forces taking place between two Ag43 α-domains, (ii) investigate the dynamics of unfolding, and (iii) address the impact of pH and external shear forces on the protein conformational and structural features. First, both gold surfaces and gold AFM-tips were functionalized by the histidine-tagged Ag43α after thiol-NTA grafting (N-ter fusion). The typical force curves corresponding to the interaction between Ag43α-functionalised gold surface and Ag43α-functionalised gold AFM-tip are reported in **Figure 2** at pH 7.4 for 100 and 3200 nm/s pulling rate conditions and in **Table 2** for intermediate values of pulling rates. The corresponding statistic distribution of the number of rupture events observed while retracting the modified-tip from the Ag43-modified surface are further displayed in **Figure 2**. The specificity of the functionalized AFM tips to

Ag43α was certified from the absence of interaction between nude gold surfaces and the modified tips (**data not shown**). **Figure 2** displays qualitatively similar retraction force curves for 100 and 3200 nm/s pulling rates with the presence of multiple adhesive events. While such event could be detected for tip to surface separation distance as large as 150 nm at 3200 nm/s pulling rate (**Figure 2b** and **Figure S4**), Ag43α uncoiling was observed over significantly shorter separation distances (40-70 nm) at 100 nm/s (**Figure 2a** and **Figure S4**). Overall, the unfolding distance appears 5 to 15 times larger than the putative size of the folded adhesin of 10 nm dimension, which reflects a significant stretchability of this protein. The structured part of the α-domain is supposedly folding as 23 complete coils with each spiral pitch containing an average of 20 amino acids ([14] and **Figure S2**). Since the minimal force required to totally and concomitantly unfold two β helical structures is above 400 pN,[37, 38] this means, theoretically, that only one β helical structure can be totally unfolded and thus a maximum of 23 rupture events should be observed by force spectroscopy measurements (note that the typical range of measured rupture force for self-associated Ag43α is *ca*. 100-200 pN, cf. **Table 2**). The average number of ruptures per force curve we found decreased from 7 ± 3 to 3 ± 2 when the pulling rate was increased from 100 to 3200 nm/s (**Figures 2c** and **2d**). These results evidenced a sequential unfolding of the interacting α-domains but with a maximum of only 5 to 10 ruptures. Basically, this suggests that the interaction between two α-domains breaks up before complete unfolding of the structures is achieved. Additionally, this result indicates that Ag43α is folded in several domains composed of multiple turns, and consequently the unfolding is sequential and takes place domain after domain and not turn after turn.

The retraction force curves depicted in **Figure 2** were further analyzed according to the Worm like Chain (WLC) model (eq 1) according to the methodology we detailed elsewhere.[39]

Briefly, this theoretical approach allowed the evaluation of several key parameters pertaining to the structural properties of Ag43α and to their homomeric interactions:

- the persistence length l_p reflecting the intrinsic flexibility of the protein;
- the contour length L_c defined as the length of the fully extended protein;
- the rupture force between two proteins;
- the number of monomers, denoted as N, for the stretched system.

The statistic distribution of the last rupture force magnitude detected in the Force volume Image (FVI) and the number of monomers extracted from the retraction force curves are collected in **Figure 3** for pulling rates of 100 and 3200 nm/s at pH 7.4. The rupture forces measured between two adhesins were not significantly modified by the pulling rate, with values of 138 ± 35 pN and 141 ± 60 pN at the two rate values adopted here. These values of rupture force measured onto model Ag43α-gold coated surfaces are comparable with those measured on living cells (**Figure S1a-3**). Moreover, the statistical analysis of N, corresponding to the number of monomers within the Ag43-Ag43 system, is bimodal, which suggests that at least 2 sub-structures were stretched during the retraction of the AFM-tip from the functionalized gold surface. We hereafter refer to N_1 and N_2 (with $N_1 < N_2$) these two values taken by N, as illustrated in Figure 3c,d. We obtained $N_1 = 422 \pm 224$ and $N_2 = 1465 \pm 272$ at 100 nm/s, and $N_1 = 418 \pm 156$ and $N_2 = 1938 \pm 711$ at 3200 nm/s (see **Table 2**). .In order to address the nature of the two types of substructures probed by force spectroscopy at 100 and 3200 nm/s and pH 7.4, we plotted in **Figure S5** the persistent length derived from WLC analysis as a function of the corresponding number of monomers N. The data clearly evidence the presence of two distinct clouds of points corresponding to the two searched substructures. In details, one may discriminate a substructure ($1000 \leq N \leq 2500$) with a persistence length l_p lower or equal to 0.15nm, and a second type of substructure ($100 \leq N \leq 1000$) with a l_p satisfying $l_p > 0.15$ nm. The former corresponds to a weak stretching of C-C

bonds and the latter to the stretching of amino acids. Indeed, the length of a C-C bond is in the range 0.12-0.15 nm, which comes to state that all persistence lengths larger than this value must necessarily correspond to amino acids. **Figure 3** shows that the bimodal distribution in terms of number of monomers does not depend on the pulling rate value. Additional experiments further show that the aforementioned bimodal distribution is not significantly affected with changing the solution pH (**Figure S6 and Table 3**).

Interestingly, a statistical switch in the respective weight distribution of the two substructures probed by force spectroscopy is observed with increasing the pulling rate from 100 to 3200 nm/s, as judged from the comparison between data collected in Figure 3c and Figure 3d. In details, the probability to observe the stretching of amino acids (N_1 ~ 500) was about 35% at 100 nm/s and increased to 57% with increasing pulling rate to 3200 nm/s. For an intermediate value of the pulling rate (400 nm/s), an iso-distribution of the two substructures is even reached regardless of the pH conditions (**Figure S6**). These results highlight the intrinsic dependence of the extent of stretching of the C-C bonds and that of the amino acids on the applied pulling rate. To put it a nutshell, a slow elongation dynamics (low pulling rate values) predominantly favors the stretching of large assemblies of amino acids (**Figure S5**) whereas faster elongation dynamics (probed at higher pulling rates) goes in pair with a stretching of smaller C-C bonds. The number of monomers corresponding to the amino acid structures is in the range 100 to 1000 (**Figure S5**). However, the complete stretching of two ß helical structures of Ag43 should lead to a number of monomers equal to 499×2 amino acids [REFERENCE]. Obviously then, the rupture forces in our experiments (≤216 pN, see Table 3) are not large enough to totally unfold simultaneously two ß helical structures, which is in agreement with the literature (250 pN at least are required to unfold two ß helical structures) (REFS).

Effect of pH and pulling rate conditions on the dynamics of Ag43 unfolding

In order to further investigate the changes in Ag43 conformation and structure during self-association of the proteins, force spectroscopy experiments were carried out at different pulling rates in the range 100-3200 nm/s with varying the solution pH (5.2, 6.1, 7.4, 8.1 and 9.2). We emphasized that the pulling rate set in the force spectroscopy experiments basically fixes the time window where the self-association modes of the Ag43α domains can be observed. Stated differently, with increasing the pulling rate, one will probe the fastest Ag43α association mode and, conversely, the lower the pulling rate, the more efficient will be the observation of the slower association mechanisms. In *fine*, varying the pulling rate allows us to modulate the measurement timescale and thus to vary the so-called Deborah number defined here as the ratio between Ag43α association timescale and measurement timescale.

Force curves similar to those given in **Figure 2** were then recorded as a function of pH and analyzed on the basis of the WLC model. A marked dependence on pH and pulling rate was detected for the maximal molecular extension denoted as L_{max} (corresponding to the maximal rupture distance of self-associated Ag43, **Figures 4a** and **4b**) and the magnitude of the last rupture force was further found to be strongly modulated by pH too (**Figure 4c** and **4d**). In details, L_{max} varied with pH according to a sigmoid-like dependence and reached plateau values at sufficiently low and large pH values. For the lowest pulling rate tested in this work (100 nm/s, **Figure 4a**), the plateau value under acid conditions was about 40 nm (corresponding pH range: 5 to 7), while the plateau reached at pH values larger than 9 was 80 nm. For higher pulling rates (3200 nm/s, **Figure 4b**), the same trend was observed, *albeit* with slightly higher plateau values reached by L_{max} for pH < 7 (50-65 nm) and pH > 9 (100-150 nm). In addition, the magnitude of the last detected rupture force depended on pH according to a bell-shaped curve regardless of the pulling rate value adopted in the experiments. At low pulling rates, a shallow maximum is obtained around neutral pH with a value of about 120-

150 pN (**Figure 4c)**. For higher pulling rates, the maximum was more pronounced with a value of 120-150 pN reached at neutral pH, similarly to the situation at lower elongation rates (**Figure 4d**). For pH higher than 8, weak ruptures forces are in line with a significant extension of the structures. For pH lower than 6, rupture forces are weak and they correspond to a minimal extension of the structures (**Figures 4a** and **4b**).

We investigated in more details the dependence of the rupture forces between Ag43 proteins on pulling rate (**Figure 5).** Over the whole range of pH conditions tested, we observed a bell-like dependence of the rupture force on pulling rate. Under the three pH conditions reported in **Figure 5**, the rupture forces gradually increased from 80-120 pN to a maximum value in the range 150-220 pN at a critical pulling rate in the range of 400-800 nm/s, and finally it somewhat decreased upon further increase of the pulling rate. This surprising feature was detected for pH values in the range 3 to 9, even though the bell-like dependence seems to be less pronounced at pH 9.2. A three-dimensional representation of the dependence of the rupture forces on pH and pulling rate, as given in **Figure S7,** can be fitted by a 3D-Gaussian form in order to estimate the pH and pulling rate conditions that are most favorable for strong Ag43 association. We found that these conditions correspond to a pH of about 7.6 and a pulling rate of 473 nm/s. The increase of the binding force between the self-associated adhesins with increasing the pulling rate is fully in line with a "catch-bond"-like mechanism where the receptor-ligand interaction is enhanced with increasing tensile mechanical force.

Macroscopic signature of Ag43-Ag43 assembly and pH dependence.

In order to evaluate the relevance - at a macroscopic scale - of the observed impact of solution pH on the self-association of Ag43 adhesins, we performed aggregation measurements over the pH range 3 to 9 on bacterial cells (*E. coli* - E2498) constitutively expressing or not the Ag43 adhesin. We report in **Figure 6** the optical density ratio OD/OD_0 that reflects the

fraction of non-aggregated (and non-settled) bacterial cells in solution. After 60 minutes, the OD/OD_0 ratio followed a marked parabola-shaped trend *versus* pH, with a pronounced minimum at pH ~ 5. After 120 and 180 minutes, the parabolic trend became strongly attenuated but a minimum in the OD/OD_0 ratio remains still clearly distinguishable at pH 5. In line with previous work from our group,[33] we verified that the OD/OD_0 ratio for the control strain (E2152) lacking the Ag43 proteins at the surface is about 1 over the time period tested in **Figure 6** regardless of the pH conditions The minimum in OD/OD_0 ratio observed for the E2498 strain should thus correspond to an optimum in aggregation as mediated by the self-association of Ag43 adhesins located on the surface of the interacting cells. In agreement with **Figure 6**, self-association of Ag43 (and therefore bacterial aggregation) is expected to be most significant at pH values close to the theoretical isoelectric point pI=4.83 of the Ag43 α-domain (calculated using http://web.expasy.org/compute_pi/). A mechanistic understanding of these results requires a molecular analysis of the Ag43 adhesins self-association modes as revealed by force spectroscopy experiments (see Discussion section). It is stressed that macroscopic measurements of the electrohydrodynamic features of bacterial cell walls[40] are not informative in that respect, as thoroughly detailed in ESI (**Figure S8**).

Discussion

The mechanical properties of bacterial adhesins play essential roles in several biophysical and interfacial processes, such as adhesion to abiotic or host cell surfaces,[41] biofilm formation,[16, 42-45] auto-aggregation and pathogenicity.[19, 46, 47] The combination of single-molecule force (SMFS) and dynamic force spectroscopies (DFS) makes it possible to address the molecular mechanisms underpinning how pathogens surface proteins contribute to host cell recognition, adhesion and infection and how processes including catch bond effect,[48] unfolding,[49] unzipping,[50] and nanospring behavior[58] come into play. Our results provided the first dynamic

and biomechanical investigation of Ag43 self-association modes under different pH and applied shear force conditions.

Mechanical behavior of Ag43 self-association

Force spectroscopy measurements are in line with the previously reported ß-helix structure of the Ag43α domain[14] essentially because our data support that Ag43α unfolding is sequential and the magnitude of the unfolding forces is in the range of 100-250 pN.[38] The latter well agrees with that given for homophilic association of BCMA0224, a prototypic trimeric autotransporter from *B. cenocepacia,* and HBHA from *M. tuberculosis*.[29, 51] The here-reported unfolding forces are also within the same range of those measured for the unfolding of single adhesins such as LapA from *P. fluorescens* and FHA from *H. influenza*.[49, 52] Interestingly, homophilic interactions of adhesins appear stronger (4- to 8-fold) than the interactions between fimbrial adhesins and their corresponding sugar ligands. Forces between 30 to 50 pN have been reported for such fimbrial adhesins/sugar interactions.[31, 53-55]

A sequential unfolding of non-fimbrial adhesins reflects the presence of several structural domains such as those recently reported for the FHA protein from *H. influenzae*.[49] In the case of Ag43α, depending on the adopted pulling rate value, we demonstrated the presence of 3 to 10 structural domains that correspond to the number of rupture events detected in the force curves. Heras *et al* demonstrated that the Ag43α domain of Ag43a in uropathogenic *E. coli* strain CFT073 exhibits a L-shaped structure consisting of a 13-rung parallel β-helix domain, followed by three rungs that bend the protein by about 110° and a C-terminal seven-rung parallel β-helix domain.[14] In this structure, 3 domains can be identified and could be further visualized from structure modeling of Ag43α in *E. coli* K-12 (see **Figure S2**): the first of these domains consists of 13 turns of 292 amino acids (green ribbon), the second contains 3 turns of 69 amino acids (red ribbon) and the last domain is composed of 7 turns in a sequence

of 137 amino acids (yellow ribbon) (see **Figure S2**). Our AFM data therefore suggest that these 3 domains contain sub-structures that are composed of several turns and that constitute independent structural segments.

The analysis of force experiments performed with increasing pulling rate revealed a catch-bond-like behavior of Ag43α. Indeed, a rise in the rupture forces from 120 up to 220 pN has been measured at pH 7.4 when the pulling rate was increased from 100 up to 1000 nm/s (**Figure 4** and **Figure 5**). In literature, "catch bond" has already been described for fimbrial adhesins (type 1, F1C and P) with an increase of the force from 30 pN up to 70 pN for pulling rate values in the range of 100 to 10000 nm/s.[56] Catch bonds may correspond to several mechanisms allowing the bond lifetime to increase with mechanical stress until a critical shear force condition is reached. Such mechanisms confer bacteria the ability to roll under low shear forces and to strongly adhere at higher shear forces, as in *e.g.* urinary flows. In our experiments, the 80% increase in the magnitude of the rupture forces between two Ag43α with increasing pulling rate from 100 to 1000 nm/s is well in agreement with that measured for the P pili from uropathogenic *E. coli*.[57, 58] This result basically indicates that auto-aggregation and adhesion of the bacteria expressing Ag43 onto Ag43-coated surfaces would be favored with increasing flow rates. Even though the molecular mechanism remains quite unclear, we think that the strong pulling rate-dependence of the adhesion force between Ag43α is a signature of catch-bond effects. This effect observed for the self-association of Ag43α domains is maximum at pH 7.4 and is strongly reduced under both low and high pH conditions (**Figure S7, Figures 4c,d**). Interestingly, this pH value where the rupture force is maximum roughly identifies with that where the curve maximal extension L_{max} *versus* pH exhibits an inflection point (**Figures 4a,b**). Overall, these results firmly demonstrate that the auto-assembly of Ag43 proteins is of a dynamic nature and that it depends on solution pH.

Is the formation of self-associated Ag43 adhesins mediated by *trans*- and/or *cis*-interactions?

Heras *et al*. have clearly identified 2 loop regions (depicted in **Figure S2** in pink and blue colors) corresponding to the so-called 1 and 1' interfaces recognized as the molecular promoters of self-recognition mechanism.[14] These authors further stated that self-association of two Ag43α domains takes place through the interfaces 1 and 1' in *trans* head-to-tail interaction acting like a molecular Velcro (**Figure 8**). Considering such an interaction configuration *via* the interfaces 1 and 1', we estimated that the maximal extension before rupture would correspond to the unfolding of the 22 amino acids sequence located before interface 1 and/or the 66 amino acids sequence located between interfaces 1 and 1', as schematized in **Figure 8**. The concomitant stretching of two 22 amino acids sequences located on both sides of interfaces 1 and 1' is also possible. Such molecular conformations should lead to maximal molecular extensions of 7, 14, 24 and 38 nm (**Figure 8**). The first and third values stem from the unfolding of only one Ag43 protein. The concomitant unfolding of the two 22 amino acid sequences would lead to 7+7=14 nm (in the case where the sequence between 1 and 1' interfaces is not unfolded) or to a maximal extension of 7+22+7=38 nm (in the case where the entire sequence along the stem of the L-shaped structure is unfolded). The unfolding mechanisms schemed in **Figure 8** result in maximal molecular extensions that are in line with those collected in **Figure 4** at sufficiently low pH values and low pulling rates (typically 100 nm/s, **Figure 4a**). This strongly suggests the occurrence of *trans*-association of Ag43α domains under such pH and pulling rate conditions.

For pH values higher than 7 and pulling rates larger than say 400 nm/s, we systemically observed a maximal extension up to 150 nm for the interacting Ag43α domains (**Figure 4**). One could argue that such large extension could be achieved from the cascade disruption of

several *trans*-associated Ag43, in a manner similar to that observed for the autotransporter SAAT adhesin Hap from *H. influenzae*.[22] However, a cascade stacking of Ag43 is not possible because, unlike Hap which is a straight solenoid, Ag43 exhibits a bend that necessarily leads to strong steric hindering of the access to the interfaces 1 and 1'. Therefore, in order to explain values as large as 150 nm for the maximal extension of Ag43α domains (**Figure 4**), it is mandatory to argue another possible configuration for Ag43α homophilic association, *i.e.* a configuration other than that previously reported from crystallography analyses.[14] We suggest that Ag43α interactions *via* the interfaces 1 and 1' following *trans*-association predominate at low to intermediate pulling rates and/or low pH (see discussion above) with as a result a moderate extension of the structure (ca 38 nm at the largest, **Figure 4**).

Since molecular extension above 38 nm cannot result from stretching of Ag43 associated according to *trans*-interactions, another type of interactions explaining the large molecular extensions observed at large pulling rate (**Figure 4b**) and to some extent at large pH values should exist. As further discussed in this section, we hypothesize that such interaction between Ag43α is faster and weaker than the *trans*-interaction detected under low pulling rate conditions. In literature, it is reported that some proteins (Als5p adhesin from *C. albicans*[59, 60], Nectin proteins[61]) may associate side-by-side in *cis*-configuration. If adopting such a configuration for Ag43α dimers where the bends of the L-shaped proteins are in opposite direction (**Figure 9a**) and further considering the sole unfolding of one out of the two interacting molecules, it can be estimated that the maximal extension expected should be around 105 nm (corresponding to 292 amino-acids). In the case where the bends of the L-shaped proteins are in the same direction (**Figure 9b**), the maximal extension is around 160 nm (corresponding to 499 amino-acids). Both values 105 and 160 nm obtained from such unfolding mechanisms very well correspond to the maximal extensions measured by AFM at

sufficiently large pH values and/or large pulling rates (**Figure 4** and **Figure S7**). To the best of our knowledge, *cis*-interactions have never been invoked for autotransporter adhesins for which self-assemblies are deemed to take place only from *trans*-interactions.[14, 22] Our results do support the occurrence of such interaction configuration. With regard to the continuous increase in maximal molecular extension with increasing pH and/or pulling rate (**Figure S7b**), it can be argued that *trans*-interactions are predominant at pH < 7 and pulling rates lower than 400 nm/s and that they lead to moderate maximal extension of the structure. Conversely, *cis*-interactions are probably the major mode of protein association at pH > 7 and at pulling rates larger than 400 nm/s, and they are in line with molecular extensions that are significantly larger than those obtained according to *trans*-interactions mode. The pH and pulling rate regimes where *cis*- and *trans*-interactions are most significant are schematized in blue and red-orange color mapping in **Figure S7b**. The buffer space defined by the green area in **Figure S7b** can be associated with the overlap between *trans*- and *cis*-interaction zones of influence. This coexistence of *cis*- and *trans*-interactions as well as the values obtained for N_1 (> 400 amino acids) suggests a possible multimerization where two or more Ag43α molecules are involved within the molecular assembly and subsequent unfolding upon retraction of the modified tip. For the sake of example, a tetrameric structure of Ag43α is possible through the *trans*-interaction between two adhesins dimers associated *via cis*-interactions (**Figure 10**). Such molecular configuration is also supported by nanogold particles-mediated observations (**Figure 1a**) that revealed the occurrence of large structures of *ca.* 200 nm, which probably corresponds to large complexes consisting of more than two Ag43α molecules.

Building mechanism and unfolding of Ag43α tetrameric structure

Multimerization of adhesins has been largely documented in literature and particularly for autotransporter adhesins such as Hap from *Haemophilus influenzae*, AidA-I from *Escherichia*

coli and YapC from *Yersinia pestis*.[62, 63] In addition, the formation of homo-tetramers starting from homo-dimers has been reported for the repair protein MutS from *Escherichia coli*[64] and also for the autotransporter adhesin BadA from *Bartonella henselae*.[65, 66] The authors stated the existence of equilibrium between dimers and tetramers and the necessity of full-length dimers interactions to achieve the tetramer formation.[64] The analysis of the modulation of the number of monomers and the maximal extension L_{max} (**Figure 3** and **Figure 4**, respectively) evidenced that molecular unfolding is quasi-completed (*i.e.* L_{max}~160nm) under restricted range of pH and pulling rates (pH~9 and pulling rate ν > 1600 nm/s, cf. **Figure S7b**) where *cis* interactions are predominant (**Figure 9**). Under such extreme ranges of pH and pulling rates, *trans*-interactions cannot take place since, in such a configuration, the only stem of the L-shaped structure of Ag43 can be unfolded leading to L_{max}~38 nm at most, in contrast to experimental data. In order to explain the continuous increase of L_{max} from ~30 nm to ~160 nm with increasing pH from 3 to 9 and/or pulling rate from 100 nm/s to 3200 nm/s, configurations intermediate between those corresponding to *trans* and *cis* interactions or combinations thereof must be envisaged. Such combinations of *trans* and *cis* interactions can lead to multimers-assemblies for Ag43, as reported for *e.g.* MutS and BadA adhesins.[64-66] In this situation, Ag43 dimers are formed by *cis*-interactions with the bends of the L-shaped structures in the opposite direction before interacting *via* interfaces 1 and 1' in a *trans*-conformation to finally achieve a tetrameric structure (**Figure 10**). The occurrence of such a structure is in line with the presence of free Ag43α molecules in excess in the solution used for surface functionalization. These free molecules can indeed form dimers with the Ag43α molecules attached to the gold-surface or to the AFM tip by virtue of rapid *cis* interaction. As discussed below, stretching of the above tetrameric structure can lead to molecular extensions between 30 nm and 210 nm, in line with extensions data collected in **Figure 4**.

The analysis of the force curves collected in the pH range 4 to 9 evidenced a strong correlation between the pH-dependent maximal unfolding of the self-associated adhesins and the corresponding rupture force (**Figure 4)**. Indeed, a systematic increase of the maximal molecular unwinding was observed with increasing pH from ~7 to 9, *i.e.* in the pH range where a maximum in the rupture forces was detected. The theoretical isoelectric points of the interfaces 1 and 1' (involved in the sole *trans* interactions) can be estimated from a proper account of the amino acids constituting these interaction regions between two sets of residues in each monomer (see **Figure S2**), with, as result, a theoretical value of 7.10. This value is close to that obtained from AFM rupture force measurements. It thus strongly suggests that this maximum in rupture force between the Ag43 adhesins is predominantly governed by the *trans*-interactions and to a lower extent by the *cis* interactions (that come into play at larger pH values). The existence of two plateau regimes for the maximal molecular extension, *i.e.* at sufficiently low and large pH values, may be further explained as follows. The low molecular extension value observed under acidic conditions could originate from the favored formation of H-bonds between the β-helices. This would necessarily increase the intra-molecular cohesion forces within the β-helices interacting in *trans*-conformation and thus reduce the stretchability of the formed dimer. The high molecular extension observed under alkaline conditions could stem from an increase of the electrostatic charges located in the β-helices. The subsequent increase in the repulsive interactions could enhance the dimer flexibility and thus increase its stretchability as compared to the low pH situation. Finally, the increase in the rupture forces with pH could be a signature of the abundance of self-associated β-helices or a signature of the switch from *trans*- to *cis*-interactions for a given dimer.

The results obtained for the maximal molecular extensions and the coexistence of *cis*- and *trans*- interactions support the existence of possible multimerization of Ag43 adhesins. The formation of a tetrameric structure composed of only Ag43α adhesins and its unfolding are

possible only on the premise that *cis*-interactions are weaker with a shorter life-time (*i.e.* accessible at large pulling rate or fast pulling dynamics) than *trans*-interactions that are stronger but with a longer life-time (slow dynamics). In view of the respective magnitude of the *cis* and *trans* interactions, the stretching of the tetramer leads to the unfolding of the dimers till breaking of the *trans*-interaction is reached. In that situation, molecular extensions between 30 nm and 210 nm may be achieved, as illustrated in **Figure 10.** Interestingly, our results suggest that Ag43α may have the properties of promoting -by *cis*-interaction- the gathering of two or more Ag43 molecules within the *E. coli* membrane (**see Figure 7**) favoring subsequent tetramers or higher-order oligomers formation between Ag43 molecules from different bacteria. This is derived from the observation of large nanogold assemblies (~ 200 nm) on cell membrane surface (**Figure 1a**). The presence of such multimeric structures promotes efficient aggregation of bacteria.

Our study illustrates how molecular effects can be correlated to macro-scale observations such as aggregation of bacteria constitutively producing Ag43 (**Figure 6**). The maximum in the interaction forces measured between Ag43 adhesins by SMFS is at pH close to 7, whereas we observed a faster bacterial aggregation at pH 5 as previously described in the literature (**Figure 6**).[11, 67, 68] This discrepancy could originate from the difference in processes probed at the nanoscale by SMFS and at the macroscopic scale in bacteria aggregation assays. The number of Ag43 molecules involved in self-association process in both situations is probably different since SMFS measurements are related to the detection of single molecules interactions while aggregation of bacteria may be the result of multiple interactions between Ag43α present at the cell surfaces of several *E. coli* cells. In the latter situation, pH-dependent interactions other than those stemming from the sole Ag43 surely mediate the rate of approach between the cells whose surface is the location of numerous other types of charged ionogenic groups.

Conclusions

In this study, the dynamics and pH-dependence of homomeric interactions between Ag43 adhesins is investigated, recalling that this protein is involved in biofilm formation and bacterial persistence mechanism. Our results support that Ag43 self-association is driven by *trans*-interactions as originally proposed by Heras *et al.* In addition, we evidenced the existence of *cis*-interactions that lead to the formation of Ag43 dimers and tetramers. Results further strongly suggest a coexistence of such *cis*- and *trans*-interactions *in vivo*. Both interactions types are expected to mediate the dynamics of Ag43 complexes formation at the surface of *E. coli* and to strengthen/enhance self-recognition interactions between bacteria. Finally, force spectroscopy experiments highlighted that Ag43 molecules have a high stretchability, and that their self-association dynamics is strongly impacted by environmental factors such as pH and magnitude of shear forces.

Materials and Methods

Bacterial strains

The *E. coli* K-12 strains used in this study are listed in **Table 1** where relevant information on their respective construction, antibiotic resistance, genotype and expression of surface appendages can be found. These isogenic strains were constructed from *Escherichia coli* MG1655 (*E. coli* genetic stock center CGSC#6300). All strains used in this study contain the *gfpmut3* gene linked to the *bla* ampicillin resistance gene (amp^R, 100 µg/ml) that makes them fluorescent, and a deletion of the *fliE* to *fliR* genes replaced by the *cat* chloramphenicol resistance gene (cm^R, 25 µg/ml). Our reference strain (E2152) has been additionally deleted for both the *fim* operon encoding type 1 fimbriae (Δ*fimA-H*::*zeo*, zeo^R 50µg/ml) and the *agn43* gene (Δ*flu*::*km*, km^R 50 µg/ml) while strain E2498 constitutively expresses the *agn43* gene

(*km*PcL*flu, km*^{R} 50 µg/ml)).[32, 43, 69]

Growth conditions and preparation for AFM experiments

Bacteria were pre-grown overnight at 37°C under agitation (150 rpm) in M63B1 minimal medium supplemented with 0.4% glucose (M63B1glu) and the appropriate antibiotic to select the strain of interest. The following day, fresh M63B1glu medium was inoculated with the overnight culture to an OD_{600} of ca 0.05 and cultivated under the same conditions until the biomass reached an OD_{600} of 0.5-0.6. Then, 2 mL of the bacterial suspension were removed and placed on a PEI-silicon wafer slide for 30 minutes. The samples were extensively rinsed with PBS solution to remove M63B1glu and placed directly into the AFM closed fluid-cell with 2 mL of PBS solution at the desired pH in the range 3 to 10.

Preparation of His-Tag Ag43α domains

The strain producing 6x-His-Tag Ag43 was constructed using λ-red linear DNA gene inactivation method with help of long primers[70, 71] followed by P1*vir* transduction. The 6x-His-tag was introduced 6 amino-acids after the sequence signal cleavage site of Ag43 in the strain TG using as a template the strain MG1655*km*PcL*flu* constitutively expressing Ag43 to create TG_*km*PcL*flu*-His.[43] We used the following primers to perform the construction:

- Ag43.500-5 5-gtttaccggtgcggtggaccggatatttg-3
- His-tag_alpha.L5 5-gtgcatcatcatcatcatcacccgggagaaaccgtgaacggcgg-3
- Ag43.ATG+500-3 5-ggcttgacgacctgccagcccttat-3
- His-tag_alpha.L3 5-ggtgatgatgatgatgatgcacaacgatgtcagcagccagcac-3.

Purification of the His-tagged α-domain of Ag43 was performed as follows: 2L culture was grown during 16h in LB medium at 37°C. Cells were harvested by low centrifugation and washed in 50 mL 0.9% NaCl, then pelleted and resuspended in 50 mL 0.5 mM Tris-HCl (pH 7.5), 75 mM NaCl. The α-domain of Ag43 was then released from the bacteria cells by heating at 60°C for 30 min and immediately cooled down on ice for 10 min prior to

centrifugation (20 min at 6000 rpm – 4°C). The detached α-domain contained in the supernatant was then purified on Ni-NTA His bind resin from Novagen and eluted with 500 mM imidazole (20 mM Tris-HCl-pH 8, 0.5M NaCl). The eluted product was immediately dialyzed over 20 mM Tris-HCl-pH 8 and concentrated up to 1.5 mg/mL using Amicon Ultra units (30KDa membrane) from Millipore. Functionality of the purified α-domain of 6x-His-Ag43 used for the functionalization of AFM tips and of Nanogold particles was evaluated by measuring the capacity of the prepared Ag43α solution to inhibit Ag43-mediated autoaggregation of the MG1655Δ*oxyR* Ag43-overproducing strain (**Figure S3**). Briefly, a 5 mL culture of MG1655Δ*oxyR* was grown in LB during 16h at 37°C, and its optical density adjusted to 3. Cells were harvested, washed once with PBS 1X and finally resuspended either in PBS 1X or in 50-100 μg/mL BSA or purified 6x-His-Ag43. The suspensions were transferred in 5 mL tubes and let to settle at room temperature for 6h and 24h for imaging. An aliquot of aggregated cells was finally transferred on a microscopy slide and cells were visualized using phase-contrast microscopy.

Bacterial Autoaggregation Assay

Aggregation assays were performed as previously described.[72] Bacteria were grown overnight at 37°C under agitation (150 rpm) in M63B1glu minimal medium. The optical density of the culture at 600 nm (OD600) was adjusted to 3.0 after centrifugation and resuspension in PBS solution at the desired pH in the range 3 to 9. 3 mL of each pH-adjusted culture was transferred to 5 mL hemolysis tubes. These tubes were incubated without agitation at room temperature. The OD600 of the upper part of each standing tube culture was determined after 60, 130 and 180 min of settling.

Chemicals and AFM-tip functionalization

Nickel sulfate ($NiSO_4$) and PBS tabs were purchased from Sigma-Aldrich (Sigma Aldrich, Saint-Quentin Fallavier, France), and used as received. NTA-thiols (HS-$(CH_2)_{11}$-EG_3-NTA) and HS-$(CH_2)_{11}$-EG_3-OH thiols were purchased from Prochimia Surfaces (ProChimia Surfaces, Sopot, Poland). PEG linkers were purchased from Hermann Gruber group (Institute of Biophysics, University of Linz, Austria). AFM-tips and gold-coated substrates were chemically modified with Ag43α using NTA-thiol linkers and His tagged Ag43α molecules following a procedure previously described [73] for the detection and uncoiling of Ag43α proteins. Gold tips (NPG-10, Bruker Nano AXS, Palaiseau, France) and gold-coated glass slides were covered by NTA-SAM after overnight incubation in a solution of NTA-thiol 0.1 mM in ethanol. Then, the tips were rinsed extensively with ethanol, dried with nitrogen and incubated 1h in 40 mM $NiSO_4$ in PBS solution. The tips were rinsed with milli-Q water, incubated with $(His)_6$-Ag43α at 0.2 mg/mL in PBS for 2h and then rinsed with PBS and stored at 4°C.

Nanogold particle functionalization and visualization

A solution of 600 µL of 0.5 mg/mL purified His-tagged Ag43α protein diluted in PBS buffer was added to 900 µL of Ni-NTA-Nanogold® (Ref #2082, 5 nm diameter, Nanoprobes, Inc. New York, USA) at 0.5 µM for 60 min at room temperature. Using a 2-fold molar excess of $(His)_6$-Ag43α significantly prevents aggregation of gold nanoparticles after functionalization. Bacterial samples prepared for AFM imaging were incubated 30 minutes with 200 µL of the functionalized nanoparticles solution. Then, the samples were rinsed extensively three times with Milli-Q water to remove excess of nanoparticles and gently dehydrated under nitrogen flow for AFM imaging.

AFM imaging, Single Molecule Force and Dynamic Force Spectroscopy measurements

AFM images were recorded with a FastScan AFM (Bruker AXS, Palaiseau, France) used in Peak Force™ tapping mode. Basically, Peak Force™ tapping mode performs a very fast force

curve at every pixel in the image. The peak interaction force in each of these force curves is then used as the imaging feedback signal. Peak Force Tapping mode modulates the Z-piezo at ~2 kHz with a default Peak Force Amplitude of 150 nm (0-peak). All values above and below this 0-peak magnitude is recorded as a Peak Force Error from which image is constructed. Force-distance curves were recorded using a MFP3D-BIO instrument (Asylum Research Technology, Atomic Force F&E GmbH, Mannheim, Germany). Conical gold coated AFM-tips were purchased from Bruker (NPG, Bruker AXS, Palaiseau, France) with spring constants of about 120-150 pN/nm. Experiments were performed in PBS at different pH values (3, 5, 7, 9 and 10) and at room temperature. Adhesion forces, conformational characteristics of the adhesins and their dynamic behavior were measured by recording Force-Volume Images (FVI) consisting of a grid of 32-by-32 force curves obtained upon approach and subsequent retraction of the tip (Single Molecule Force Spectroscopy for SMFS experiments) at a loading rate in the range 10^4-10^5 pN/s (variable retraction speed for DFS experiments).

In the SMFS experiments, the adhesins located on the gold-surfaces and on the biological samples were stretched upon removal of the chemically modified AFM tip away from the surface (see **Figure S2**). The obtained force *versus* distance curves were then analyzed on the basis of the WLC (Worm Like Chain) model. This model is the most suitable and frequently used to describe the extension of polypeptides.[74, 75] The extension z of a macromolecule is related to the retraction force F_{adh} *via* (eq.1):

$$F_{\mathrm{adh}}(z) = -\frac{k_B T}{l_p}\left[\frac{z}{L_c} + 4\left(1-\frac{z}{L_c}\right)^{-2} - \frac{1}{4}\right] \qquad \text{(eq.1)}$$

where the persistence length l_p is a direct measure of the chain stiffness, L_c is the total contour length of the biomacromolecule and k_B is the Boltzmann constant.

The number of monomers in the polypeptide chains was then derived from the following equation (eq.2):

$$N = \frac{L_c}{l_p} \qquad \text{(eq.2)}$$

All the FVI were analyzed by mean of an automatic Matlab algorithm described elsewhere.[39]

Electronic Supplementary Information (ESI)

Electronic Supplementary Information (ESI) available: This material is available free of charge via the Internet at http://www.rsc.org/.

References

1. R. G. Gerlach and M. Hensel, *Int. J. Med. Microbiol.*, 2007, **297**, 401-415.

2. R. Fronzes, H. Remaut and G. Waksman, *EMBO J.*, 2008, **27**, 2271-2280.

3. P. Klemm, R. M. Vejborg and O. Sherlock, *Int. J. Med. Microbiol.*, 2006, **296**, 187-195.

4. J. C. Leo, I. Grin and D. Linke, *Philos. Trans. R. Soc. B-Biol. Sci.*, 2012, **367**, 1088-1101.

5. I. Benz and M. A. Schmidt, *Infect. Immun.*, 1989, **57**, 1506-1511.

6. E. A. Elsinghorst and J. A. Weitz, *Infect. Immun.*, 1994, **62**, 3463-3471.

7. B. Diderichsen, *J. Bacteriol.*, 1980, **141**, 858-867.

8. P. Owen, in *Electroimmunochemical analysis of membrane proteins*, ed. JB, Elsevier Science Publishing, Inc. , Amsterdam, 1983, pp. 347–373.

9. T. J. Wells, M. Totsika and M. A. Schembri, *Microbiology-(UK)*, 2010, **156**, 2459-2469.

10. J. B. Kaper, J. P. Nataro and H. L. T. Mobley, *Nat. Rev. Microbiol.*, 2004, **2**, 123-140.

11. P. Klemm, L. Hjerrild, M. Gjermansen and M. A. Schembri, *Mol. Microbiol.*, 2004, **51**, 283-296.

12. P. Caffrey and P. Owen, *J. Bacteriol.*, 1989, **171**, 3634-3640.

13. M. W. Van der Woude and I. R. Henderson, *Annu. Rev. Microbiol.*, 2008, **62**, 153-169.

14. B. Heras, M. Totsika, K. M. Peters, J. J. Paxman, C. L. Gee, R. J. Jarrott, M. A. Perugini, A. E. Whitten and M. A. Schembri, *Proc Natl Acad Sci. USA*, 2014, **111**, 457-462.

15. H. Hasman, T. Chakraborty and P. Klemm, *J. Bacteriol.*, 1999, **181**, 4834-4841.

16. C. Beloin, A. Roux and J. Ghigo, *Curr. Top. Microbiol.*, 2008, **322**, 249-289.

17. P. N. Danese, L. A. Pratt, S. L. Dove and R. Kolter, *Mol. Microbiol.*, 2000, **37**, 424-432.

18. I. R. Henderson, M. Meehan and P. Owen, in *Mechanisms in the Pathogenesis of Enteric Diseases*, eds. P. S. Paul, D. H. Francis and D. A. Benfield, 1997, vol. 412, pp. 349-355.

19. G. C. Ulett, J. Valle, C. Beloin, O. Sherlock, J. M. Ghigo and M. A. Schembri, *Infect. Immun.*, 2007, **75**, 3233-3244.

20. G. G. Anderson, J. J. Palermo, J. D. Schilling, R. Roth, J. Heuser and S. J. Hultgren, *Science*, 2003, **301**, 105-107.

21. S. Fexby, T. Bjarnsholt, P. O. Jensen, V. Roos, N. Hoiby, M. Givskov and P. Klemm, *Infect. Immun.*, 2007, **75**, 30-34.

22. G. Y. Meng, N. Spahich, R. Kenjale, G. Waksman and J. W. St Geme, *EMBO J.*, 2011, **30**, 3864-3874.

23. Y. F. Dufrêne, *Nature Reviews: Microbiology*, 2004, **2**, 451-460.

24. Y. F. Dufrêne, *Nat. Protoc.*, 2008, **3**, 1132-1138.

25. G. Francius, S. Lebeer, D. Alsteens, L. Wildling, H. J. Gruber, P. Hols, S. De Keersmaecker, J. Vanderleyden and Y. F. Dufrêne, *ACS Nano*, 2008, **2**, 1921-1929.

26. V. Dupres, D. Alsteens, G. Andre and Y. F. Dufrene, *Trends Microbiol.*, 2010, **18**, 397-405.

27. P. Hinterdorfer and Y. F. Dufrêne, *Nat. Methods*, 2006, **3**, 347-355.

28. D. Alsteens, M. C. Garcia, P. N. Lipke and Y. F. Dufrêne, *Proc. Natl. Acad. Sci. USA*, 2010, **107**, 20744-20749.

29. S. El-Kirat-Chatel, D. Mil-Homens, A. Beaussart, A. M. Fialho and Y. F. Dufrêne, *Mol. Microbiol.*, 2013, **89**, 649-659.

30. I. E. Ivanov, C. D. Boyd, P. D. Newell, M. E. Schwartz, L. Turnbull, M. S. Johnson, C. B. Whitchurch, G. A. O'Toole and T. A. Camesano, *Res. Microbiol.*, 2012, **163**, 685-691.

31. A. Jacquot, C. Sakamoto, A. Razafitianamaharavo, C. Caillet, J. Merlin, A. Fahs, J. M. Ghigo, C. Beloin, J. F. L. Duval and G. Francius, *J. Biomed. Nanotechnol.*, 2014, **10**, 3361-3372.

32. G. Francius, P. Polyakov, J. Merlin, Y. Abe, J. M. Ghigo, C. Merlin, C. Beloin and J. F. L. Duval, *PLoS One*, 2011, **6**, e20066.

33. A. Chauhan, C. Sakamoto, J. M. Ghigo and C. Beloin, *PLoS One*, 2013, **8**, e73568.

34. H. Hasman, M. A. Schembri and P. Klemm, *J. Bacteriol.*, 2000, **182**, 1089-1095.

35. S. Jain, P. van Ulsen, M. A. Schmidt, R. Fernandez, J. Tommassen and M. B. Goldberg, *J. Bacteriol.*, 2006, **188**, 4841-4850.

36. D. Alsteens, V. Dupres, S. A. Klotz, N. K. Gaur, P. N. Lipke and Y. F. Dufrene, *ACS Nano*, 2009, **3**, 1677-1682.

37. J. P. Junker and M. Rief, *Proc. Natl. Acad. Sci. USA*, 2009, **106**, 14361-14366.

38. M. Rief, J. Pascual, M. Saraste and H. E. Gaub, *J. Mol. Biol.*, 1999, **286**, 553-561.

39. P. Polyakov, C. Soussen, J. B. Duan, J. F. L. Duval, D. Brie and G. Francius, *PLoS One*, 2011, **6**, e18887.

40. J. F. L. Duval and F. Gaboriaud, *Curr. Opin. Colloid Interface Sci.*, 2010, **15**, 184-195.

41. R. J. T. Emerson and T. A. Camesano, *Appl. Environ. Microbiol.*, 2004, **70**, 6012-6022.

42. M. Klausen, A. Heydorn, P. Ragas, L. Lambertsen, A. Aaes-Jorgensen, S. Molin and T. Tolker-Nielsen, *Mol. Microbiol.*, 2003, **48**, 1511-1524.

43. S. Da Re, B. Le Quere, J. M. Ghigo and C. Beloin, *Appl. Environ. Microbiol.*, 2007, **73**, 3391-3403.

44. N. A. Ledeboer and B. D. Jones, *J. Bacteriol.*, 2005, **187**, 3214-3226.

45. K. Jonas, H. Tomenius, A. Kader, S. Normark, U. Romling, L. M. Belova and O. Melefors, *BMC Microbiol.*, 2007, **7**, 9.

46. L. Craig, M. E. Pique and J. A. Tainer, *Nat. Rev. Microbiol.*, 2004, **2**, 363-378.

47. A. N. Mabbett, G. C. Ulett, R. E. Watts, J. J. Tree, M. Totsika, C. L. Y. Ong, J. M. Wood, W. Monaghan, D. F. Looke, G. R. Nimmo, C. Svanborg and M. A. Schembri, *Int. J. Med. Microbiol.*, 2009, **299**, 53-63.

48. P. Aprikian, G. Interlandi, B. A. Kidd, I. Le Trong, V. Tchesnokova, O. Yakovenko, M. J. Whitfield, E. Bullitt, R. E. Stenkamp, W. E. Thomas and E. V. Sokurenko, *PLoS Biol.*, 2011, **9**, e1000617.

49. D. Alsteens, N. Martinez, M. Jamin and F. Jacob-Dubuisson, *PLoS One*, 2013, **8**, e73572.

50. D. J. Muller, W. Baumeister and A. Engel, *Proc. Natl. Acad. Sci. USA*, 1999, **96**, 13170-13174.

51. C. Verbelen, D. Raze, F. Dewitte, C. Locht and Y. F. Dufrene, *J. Bacteriol.*, 2007, **189**, 8801-8806.

52. S. El-Kirat-Chatel, A. Beaussart, C. D. Boyd, G. A. O'Toole and Y. F. Dufrêne, *ACS Chem. Biol.*, 2014, **9**, 485-494.

53. J. E. Klinth, M. Castelain, B. E. Uhlin and O. Axner, *PLoS One*, 2012, **7**, e38548.

54. M. Castelain, S. Ehlers, J. Klinth, S. Lindberg, M. Andersson, B. E. Uhlin and O. Axner, *Eur. Biophys. J. Biophy.*, 2011, **40**, 305-316.

55. M. Castelain, A. E. Sjostrom, E. Fallman, B. E. Uhlin and M. Andersson, *Eur. Biophys. J. Biophy.*, 2010, **39**, 1105-1115.

56. O. Axner, M. Andersson, O. Bjornham, M. Castelain, J. Klinth, E. Koutris and S. Schedin, in *Bacterial Adhesion: Chemistry, Biology and Physics*, eds. D. Linke and A. Goldman, Springer-Verlag Berlin, Berlin, 2011, vol. 715, pp. 301-313.

57. M. Andersson, E. Fallman, B. E. Uhlin and O. Axner, *Biophys. J.*, 2006, **91**, 2717-2725.

58. O. Bjornham, H. Nilsson, M. Andersson and S. Schedin, *Eur. Biophys. J. Biophy.*, 2009, **38**, 245-254.

59. A. Beaussart, D. Alsteens, S. El-Kirat-Chatel, P. N. Lipke, S. Kucharikova, P. Van Dijck and Y. F. Dufrene, *ACS Nano*, 2012, **6**, 10950-10964.

60. D. Alsteens, A. Beaussart, S. Derclaye, S. El-Kirat-Chatel, H. R. Park, P. N. Lipke and Y. F. Dufrene, *Anal Methods*, 2013, **5**, 3657-3662.

61. O. J. Harrison, J. Vendome, J. Brasch, X. Jin, S. Hong, P. S. Katsamba, G. Ahlsen, R. B. Troyanovsky, S. M. Troyanovsky, B. Honig and L. Shapiro, *Nat. Struct. Mol. Biol.*, 2012, **19**, 906-915.

62. A. Lyskowski, J. C. Leo and A. Goldman, *Adv. Exp. Med. Biol.*, 2011, **715**, 143-158.

63. S. Felek, M. B. Lawrenz and E. S. Krukonis, *Microbiology-(UK)*, 2008, **154**, 1802-1812.

64. F. S. Groothuizen, A. Fish, M. V. Petoukhov, A. Reumer, L. Manelyte, H. H. K. Winterwerp, M. G. Marinus, J. H. G. Lebbink, D. I. Svergun, P. Friedhoff and T. K. Sixma, *Nucleic Acids Res.*, 2013, **41**, 8166-8181.

65. P. O. Kaiser, D. Linke, H. Schwarz, J. C. Leo and V. A. Kempf, *Cell. Microbiol.*, 2012, **14**, 198-209.

66. M. D. Hartmann, O. Ridderbusch, K. Zeth, R. Albrecht, O. Testa, D. N. Woolfson, G. Sauer, S. Dunin-Horkawicz, A. N. Lupas and B. H. Alvarez, *Proc. Natl. Acad. Sci. USA*, 2009, **106**, 16950-16955.

67. O. Sherlock, R. M. Vejborg and P. Klemm, *Infect. Immun.*, 2005, **73**, 1954-1963.

68. O. Sherlock, M. A. Schembri, A. Reisner and P. Klemm, *J. Bacteriol.*, 2004, **186**, 8058-8065.

69. C. G. Korea, R. Badouraly, M. C. Prévost, J. M. Ghigo and C. Beloin, *Environ. Microbiol.*, 2010, **12**, 1957-1977.

70. M. K. Chaveroche, J. M. Ghigo and C. d'Enfert, *Nucleic Acids Res.*, 2000, **28**, n°22e97.

71. A. Derbise, B. Lesic, D. Dacheux, J. M. Ghigo and E. Carniel, *FEMS Immunol. Med. Microbiol.*, 2003, **38**, 113-116.

72. A. Roux, C. Beloin and J. M. Ghigo, *J. Bacteriol.*, 2005, **187**, 1001-1013.

73. V. Duprès, F. D. Menozzi, C. Locht, B. H. Clare, N. L. Abbott, S. Cuenot, C. Bompard, D. Raze and Y. F. Dufrêne, *Nat. Methods*, 2005, **2**, 515-520.

74. H. Wei and T. G. M. van de Ven, *Appl. Spectrosc. Rev.*, 2008, **43**, 111-133.

75. F. Rico, A. Rigato, L. Picas and S. Scheuring, *J. Nanobiotechnol.*, 2013, **11**, S3.

76. J. M. Ghigo, *Nature*, 2001, vol. 412, pp. 442-445.

77. J. M. Ghigo, *Nature*, 2001, **412**, 442-445.

78. M. Chaveroche, J. Ghigo and C. d'Enfert, *Nucleic Acids Research*, 2000, **28**, e97.

76 et 77 sont la meme reference !!!!!!!!!!!!!!!!!!!!!!!!!!!!!!!!

TABLES

Table 1. Strains and plasmids used in this work.

Strain or plasmid	Relevant genotypic and phenotypic characteristics	Source or reference
Strains		
TG	TG1 cured of the F plasmid, proline auxotroph	77
MG1655Δ*oxyR*	MG1655 deleted for *oxyR*, constitutive production of Ag43, Km^R	72
MG1655*km*PcL*flu*	*flu* (*agn43*) gene placed under the control of the *km*PcLrbs cassette λP_R promoter, constitutive Ag43 production, Km^R	43
TG_*km*PcL*flu*-His	6x-His tag placed 6 amino-acids after the Ag43 signal sequence cleavage site in strain TG with constitutive expression of *flu* (*agn43*), Km^R	This study
E2152	MG1655_*gfp*_Δ*fliE-R*::*cat*_Δ*flu*::Km_Δ*fimAICDFGH*::*zeo*, GFP+, no flagella, no Ag43 protein, no type 1 fimbriae, Amp^R, Cm^R, Km^R, Zeo^R	32
E2498	MG1655_*gfp*_Δ*fliE-R*::*cat*_Δ*fimAICDFGH*::*zeo*_*km*PcL*flu*, GFP+, no flagella, no type 1 fimbriae, constitutive Ag43, Amp^R, Cm^R, Km^R, Zeo^R	32
Plasmids		
pKOBEG	pSC101 ts (replicates at 30°C), araC, arabinose-inducible λredγβα operon , Cm^R	78

Table 2.

Values of the conformational parameters (number of rupture events per force curve, persistence length, contour length, rupture force and number of monomers) derived from WLC modeling (eq 1) at pH 7.4 for various retraction rates (indicated). Data were extracted from a 5 μm × 5 μm Force Volume Image (FVI) consisting of 1024 force curves recorded at pH 7 over the range of pulling rate 100 - 3200 nm/s. The double entries for persistence length, contour length and number of monomers originate from the bimodal distribution issued from

the statistical analysis of **Figure 3** and **Figure S4**. * corresponds to the average value of N_1 and ** corresponds to the average value of N_2. See text for further details.

Worm Like Chain model (pH 7.4)				
Retraction rate (nm/s)	100	400	1600	3200
Number of ruptures	7 ± 2	7 ± 3	4 ± 2	4 ± 2
Persistence length (nm)	0.04 ± 0.03 0.15 ± 0.06	0.07 ± 0.04 0.16 ± 0.05	0.07 ± 0.05 0.15 ± 0.07	0.04 ± 0.03 0.13 ± 0.08
Contour length (nm)	13.71 ± 5.93 41.09 ± 21.54	26.75 ± 13.41 49.31 ± 19.16	31.03 ± 17.33 71.45 ± 22.28	36.25 ± 11.08 94.67 ± 19.62
Rupture forces (pN)	138 ± 35	216 ± 47	211 ± 82	141 ± 60
Number of monomers	422 ± 224* 1465 ± 272**	385 ± 262* 1495 ± 412 **	407 ± 252* 1376 ± 427**	418 ± 156* 1938 ± 711**

Table 3.

Values of the number of monomers derived from WLC modelling (eq 1) for various pH values at a pulling rate of 400 nm/s. Data were extracted from a 5 μm × 5 μm Force Volume Image (FVI) consisting of 1024 force curves recorded over a pH range of 5-9 for a pulling rate of 400 nm/s.

Worm Like Chain model (v = 400 nm/s)					
pH	5.2	6.1	7.4	8.1	9.2
N_1	338 ± 207 (49)	347 ± 236 (49)	385 ± 262 (49)	341 ± 216 (47)	418 ± 286 (44)
N_2	1495 ± 242 (51)	1621 ± 293 (51)	1495 ± 412 (51)	1493 ± 403 (53)	1638 ± 711 (56)

List of Figures

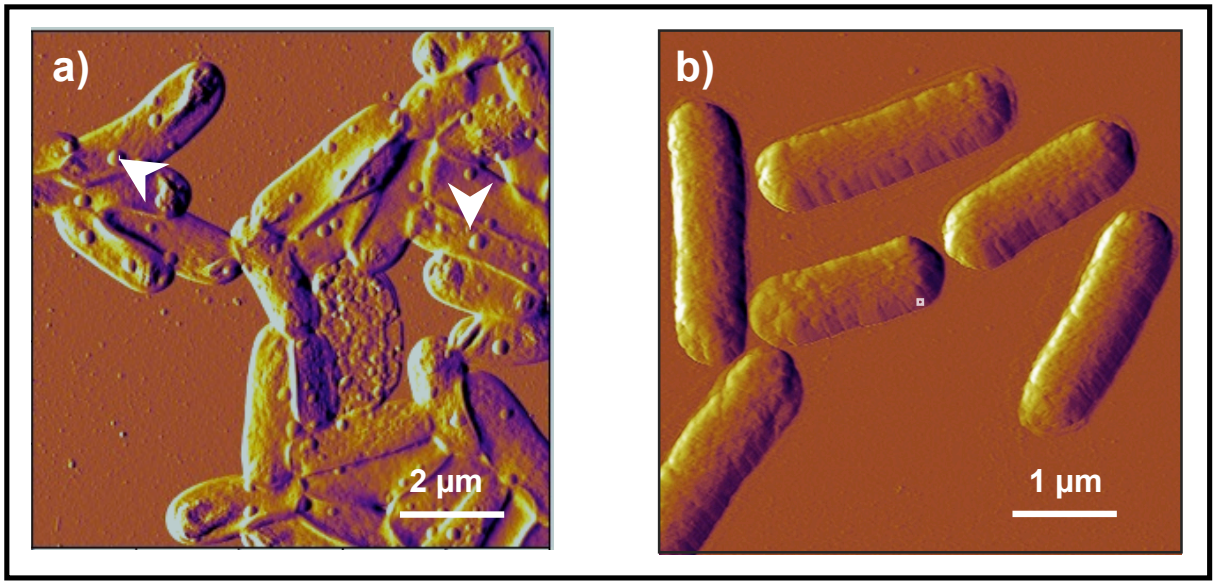

Figure 1. Morphological analyses and nanogold-mediated detection of Ag43 produced by *E. coli*.

Nanogold-mediated detection of cell surface Ag43 by AFM. Images were carried out in air after slight dehydration of the sample. E2498 Ag43 constitutive producer bacterial cells (a) and E2152 non Ag43 producer bacteria (negative control strain) (b) were immobilized onto a PEI coated substrate, exposed for 1 hour to a solution containing Ag43α-functionalized nanogold particles and then extensively rinsed with PBS.

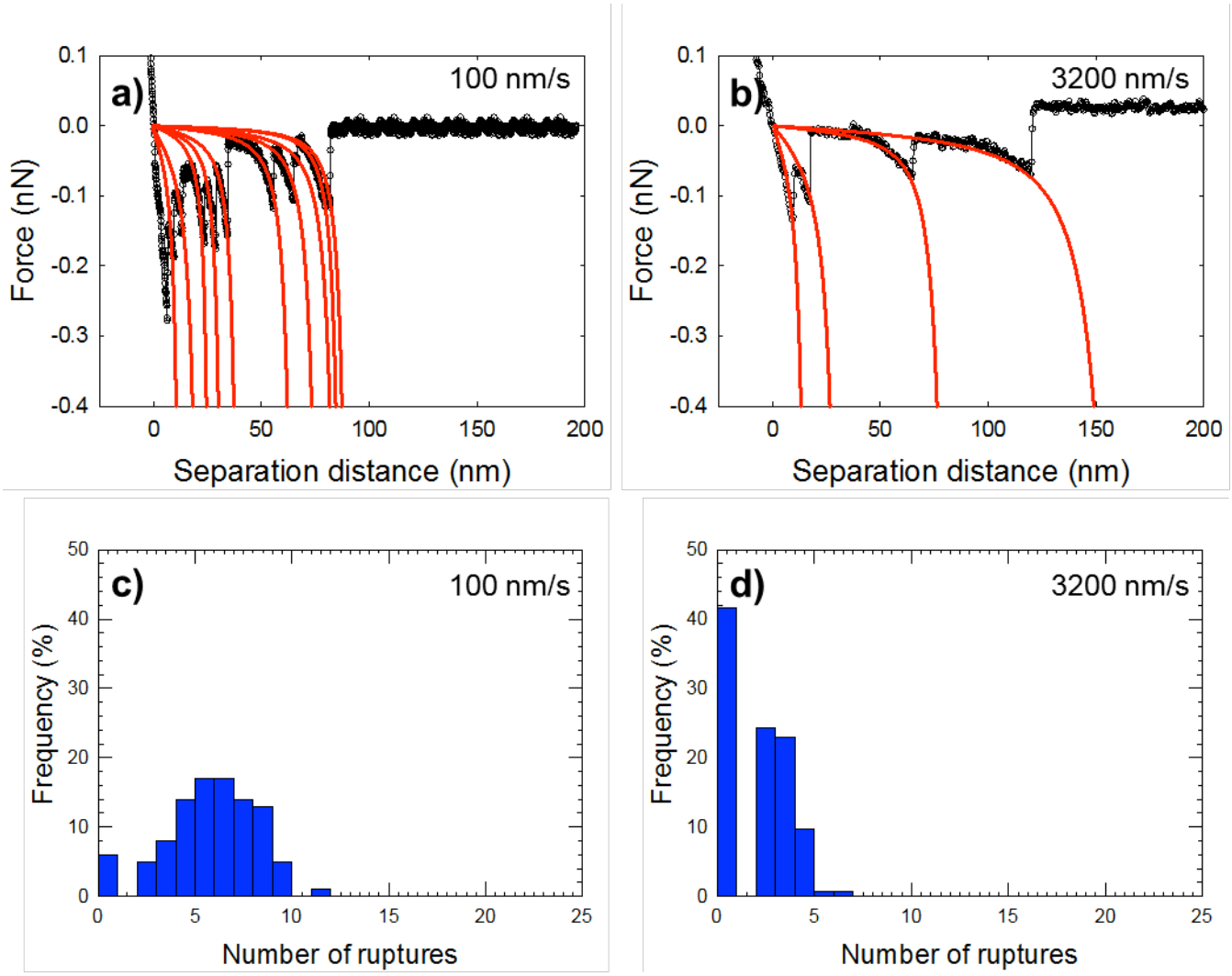

Figure 2. Retraction force curves and statistical analysis of the rupture events.

(a, b) Typical force-curves corresponding to the molecular unfolding of Ag43 α-domains on model gold surfaces for retraction speeds of 100 nm/s (panel a) and 3200 nm/s (panel b) at pH 7.4. Black circles correspond to experimental retraction force curves and red lines correspond to WLC theoretical fitting. (c, d) Statistical distribution of the number of ruptures events per force curve for pulling rate of 100 nm/s (panel c) and 3200 nm/s (panel d) at pH 7.4.

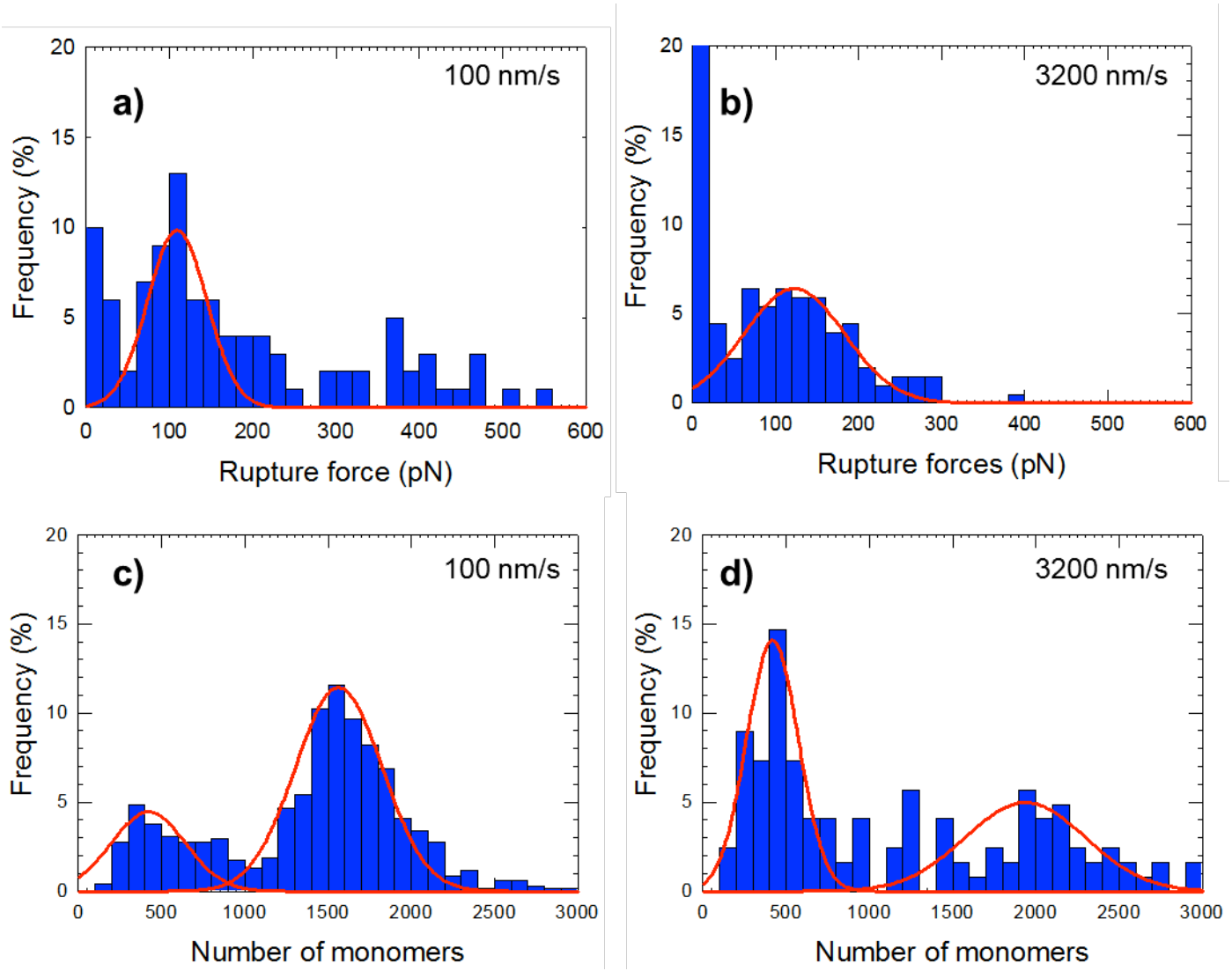

Figure 3. Adhesion forces and statistical analysis from WLC modeling.

(a, b) Statistical distribution of the rupture forces measured between Ag43 α-domains for pulling rates of 100 nm/s (panel a) and 3200 nm/s (panel b) at pH 7.4. (c, d) Statistical distribution of *N*, the number of monomers detected during the protein unfolding. Values were obtained from WLC modeling of the force curves for pulling rates of 100 nm/s (panel c) and 3200 nm/s (panel d) at pH 7.4.

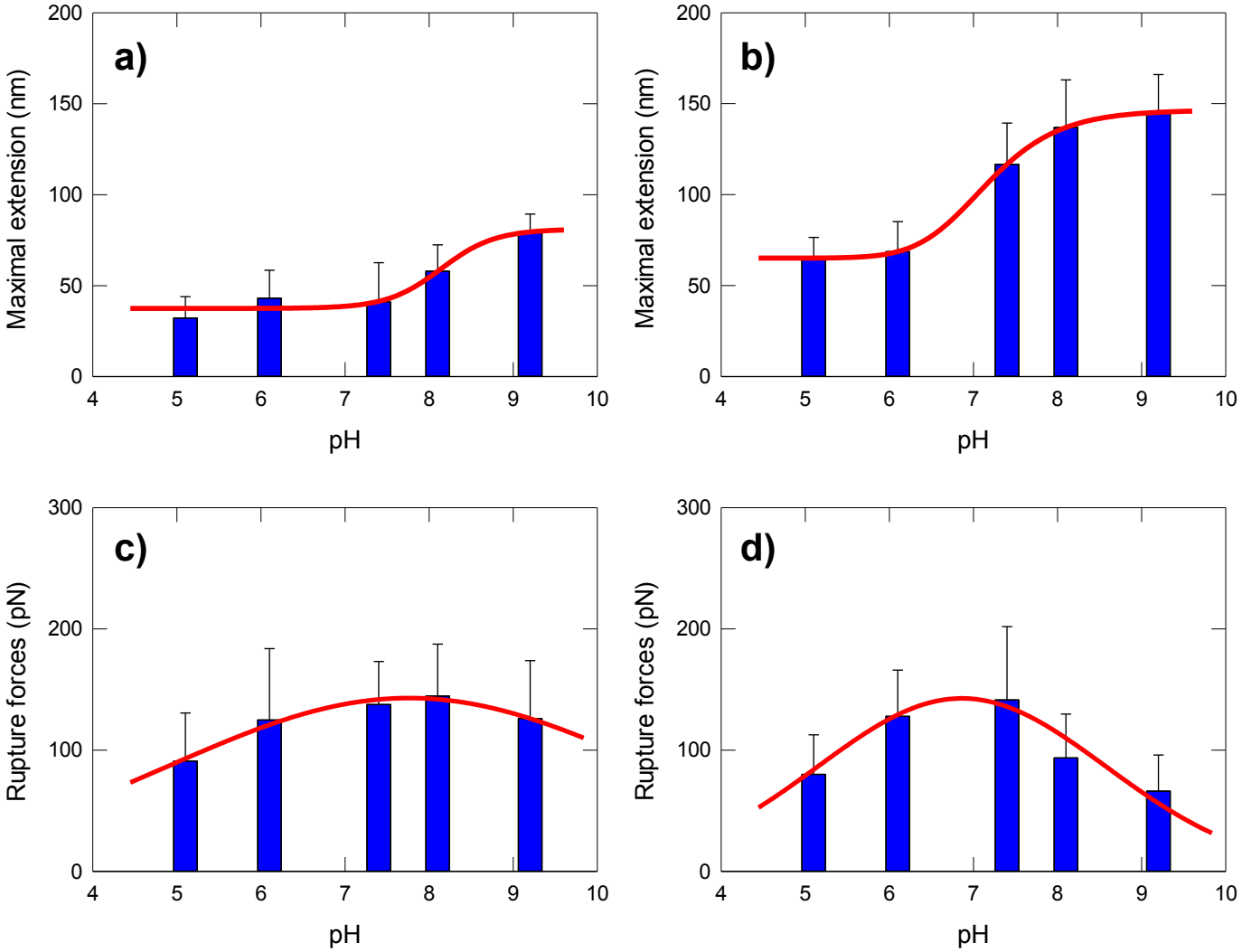

Figure 4. Dependence of the maximal molecular extension and rupture force on solution pH and pulilng rate value.

(a, b) Evolution with pH of the average maximal molecular extension of Ag43 self-associated adhesins measured by SMFS at 100 nm/s (panel a) and 3200 nm/s (panel b). The average maximal extensions were calculated from the statistic distributions of the last rupture distances derived from the whole retraction force curves at pulling rates of 100 nm/s and 3200 nm/s. (c, d) Evolution with pH of the average rupture forces of Ag43 self-associated adhesins measured by SMFS. The average rupture forces were calculated from the whole retraction force curves at pulling rates of 100 nm/s (panel c) and 3200 nm/s (panel d).

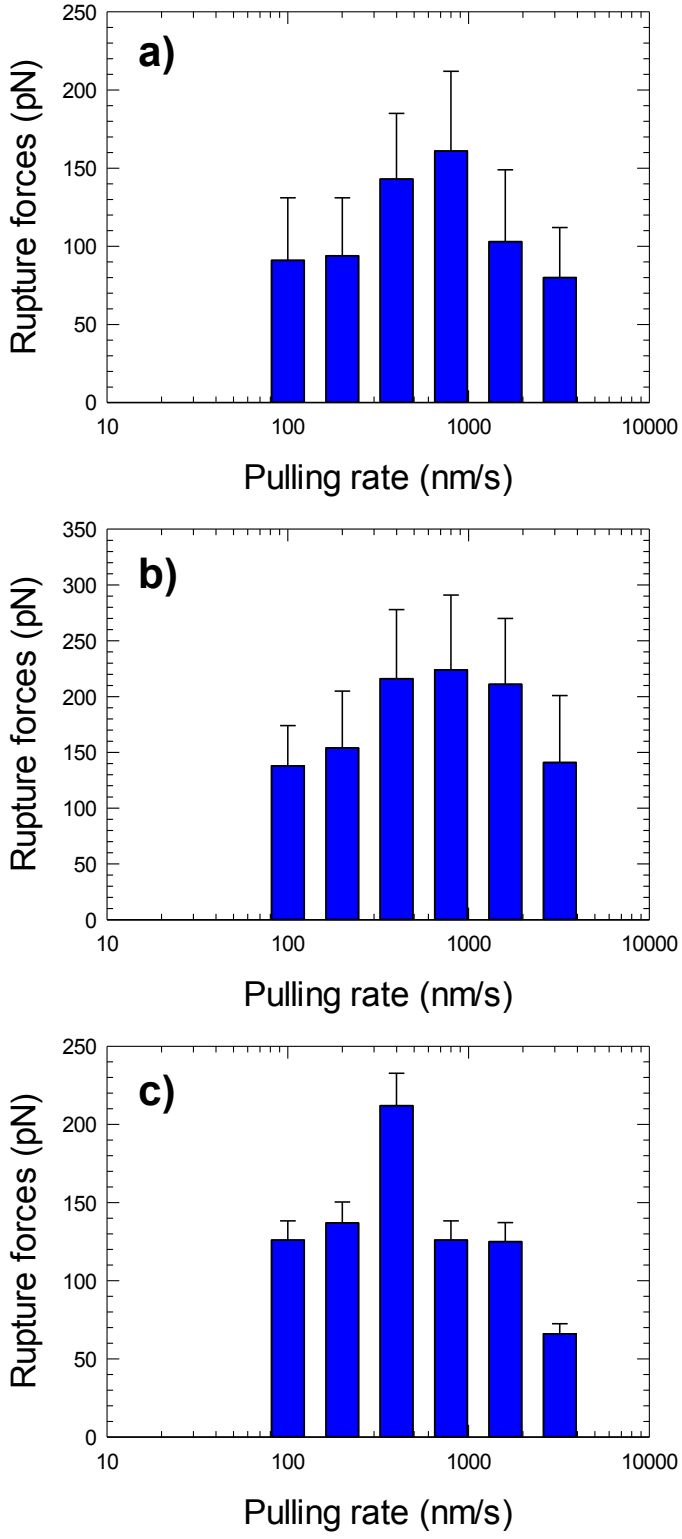

Figure 5. Effect of the solution pH on the catch-bond-like behavior of Ag43α.

Evolution of the rupture forces (dissociation) of self-associated Ag43 α-domains measured by SMFS as a function of pulling rate at pH 5.2 (a), 7.4 (b) and 9.2 (c).

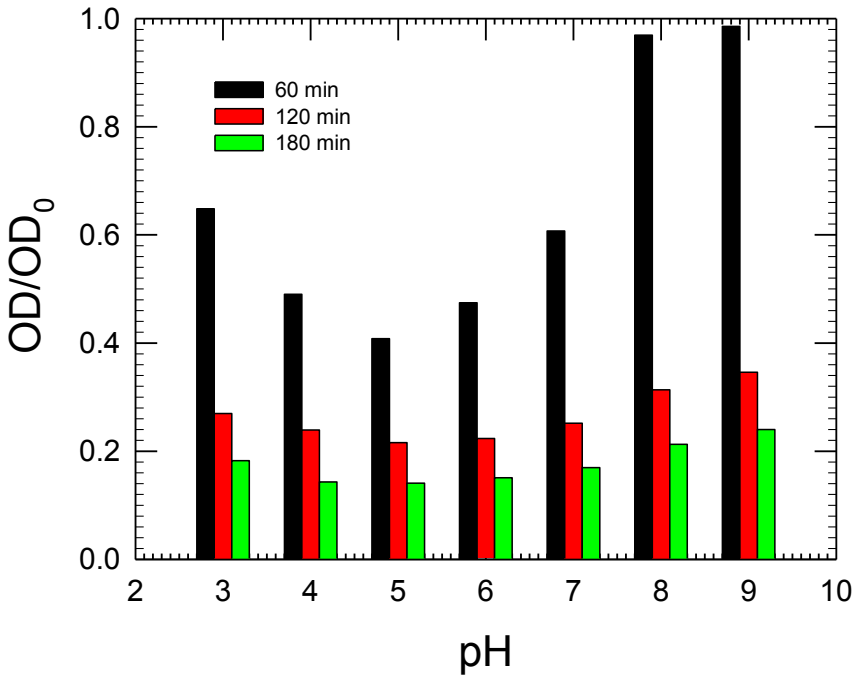

Figure 6. Effect of pH on the kinetics of Ag43-mediated *E. coli* auto-aggregation.

Auto-aggregation profiles for the E2498 strain performed over the pH range 3-9. Optical density (OD) values were measured after 60 min, 120 min and 180 min and normalized by OD values at t = 0 min. In line with previous work from our group,[33] we verified that the OD/OD_0 ratio for the control strain (E2152) lacking the Ag43 proteins at the surface is about 1 over the time period tested in Figure 6 regardless of the pH conditions

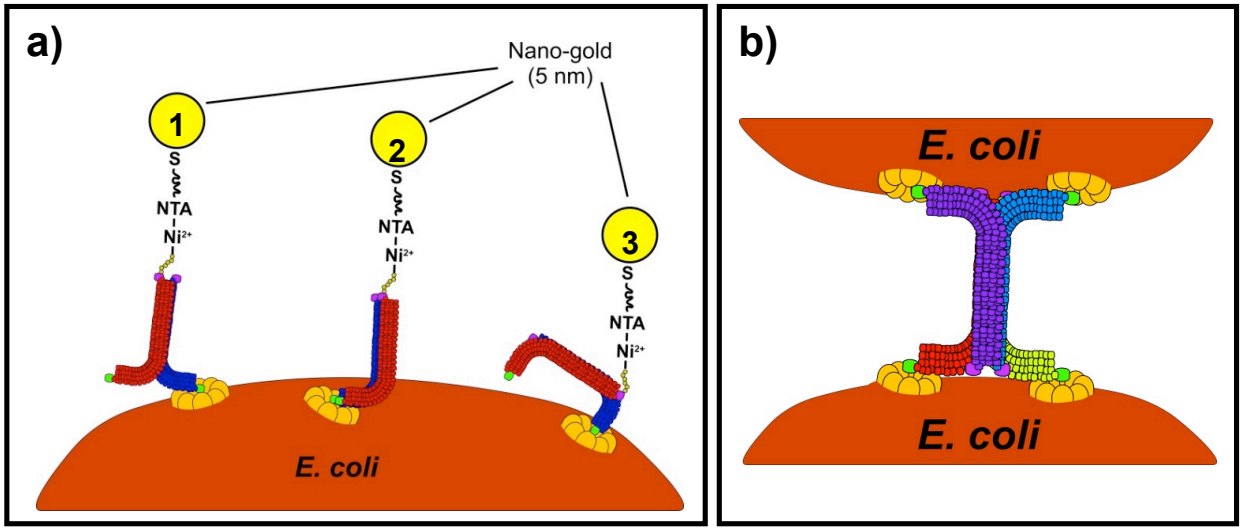

Figure 7. Schematic representation of possible *cis*- and *trans*-conformation of adhesins interactions for explaining nanogold detection and SMFS experiments.

Schematic representations of the possible conformations of nanogold particles attached onto bacterial cells (a) and the multiple Ag43α self-association between two bacteria (b). Conformations 1 and 2 correspond to Ag43α dimerization through *cis*-interactions (the bends of the L-shaped proteins are either along the same or opposite direction). Conformation 3 illustrates the Ag43α self-association mediated by the *trans*-interaction (L-shaped adhesins are interacting like a molecular Velcro with a head-to-tail geometry).

.

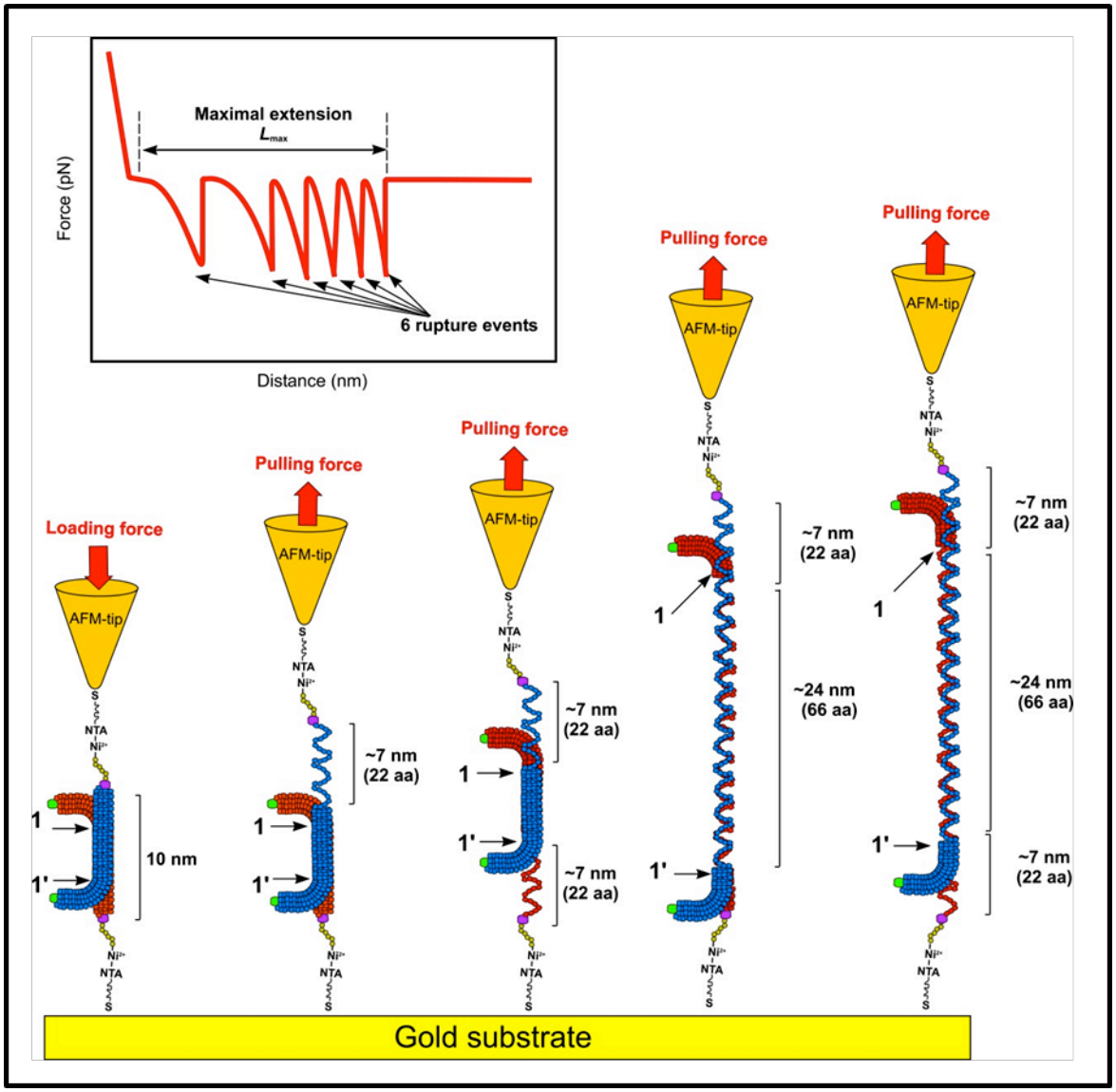

Figure 8. Schematic representation of the unfolding of *trans*-associated Ag43α (predominant at sufficiently low values of solution pH and pulling rate). Representation of the envisaged unfolding of *trans*-associated Ag43α dimers formed during force spectroscopy experiments.

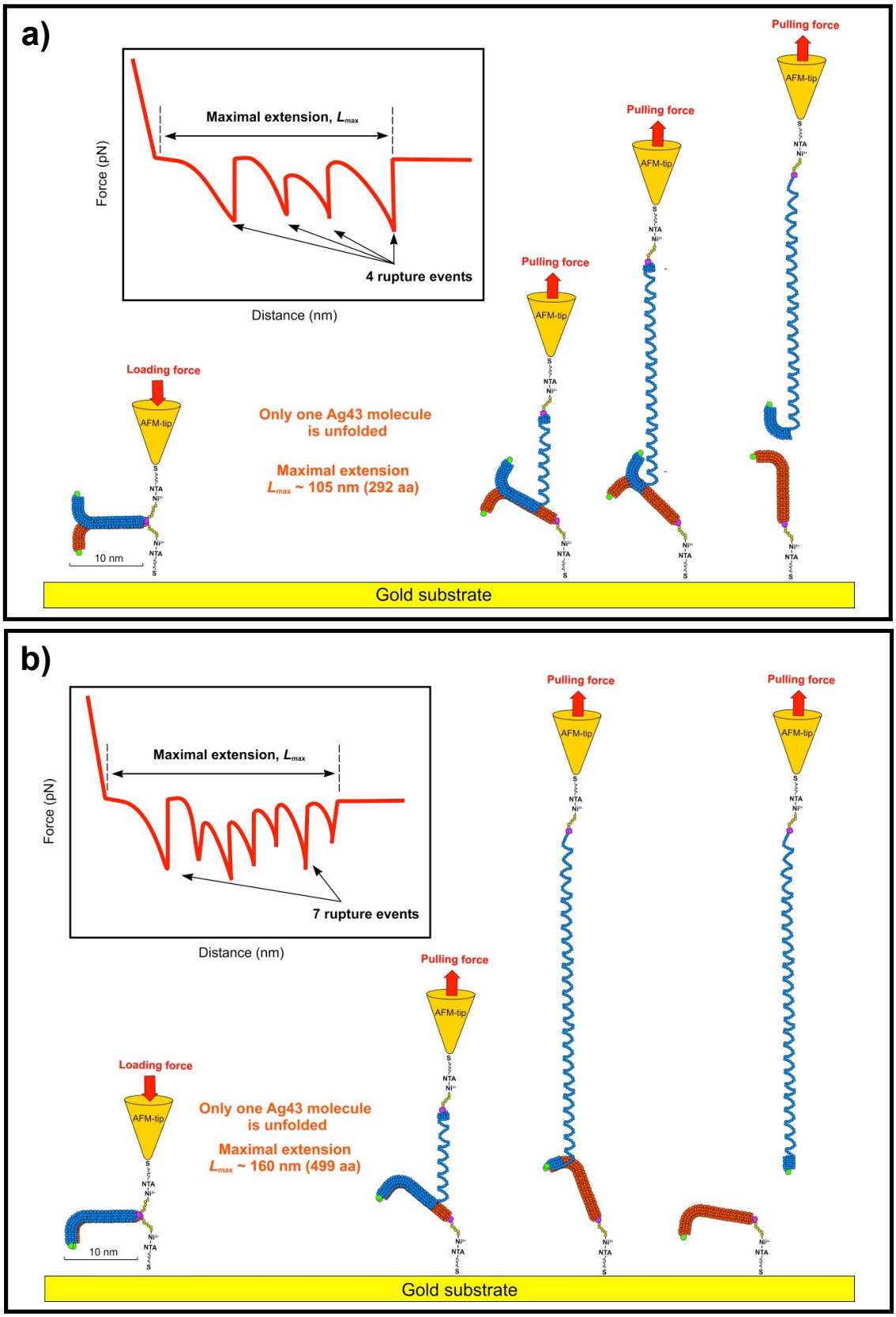

Figure 9. Schematic representation of the unfolding of *cis*-associated Ag43α (predominant at sufficiently large values of solution pH and pulling rate).

Representation of the envisaged formation and unfolding of a dimer of Ag43α formed by *cis*-interactions. The bends of the twisted L-shaped proteins are in opposite direction a) or along the same direction b).

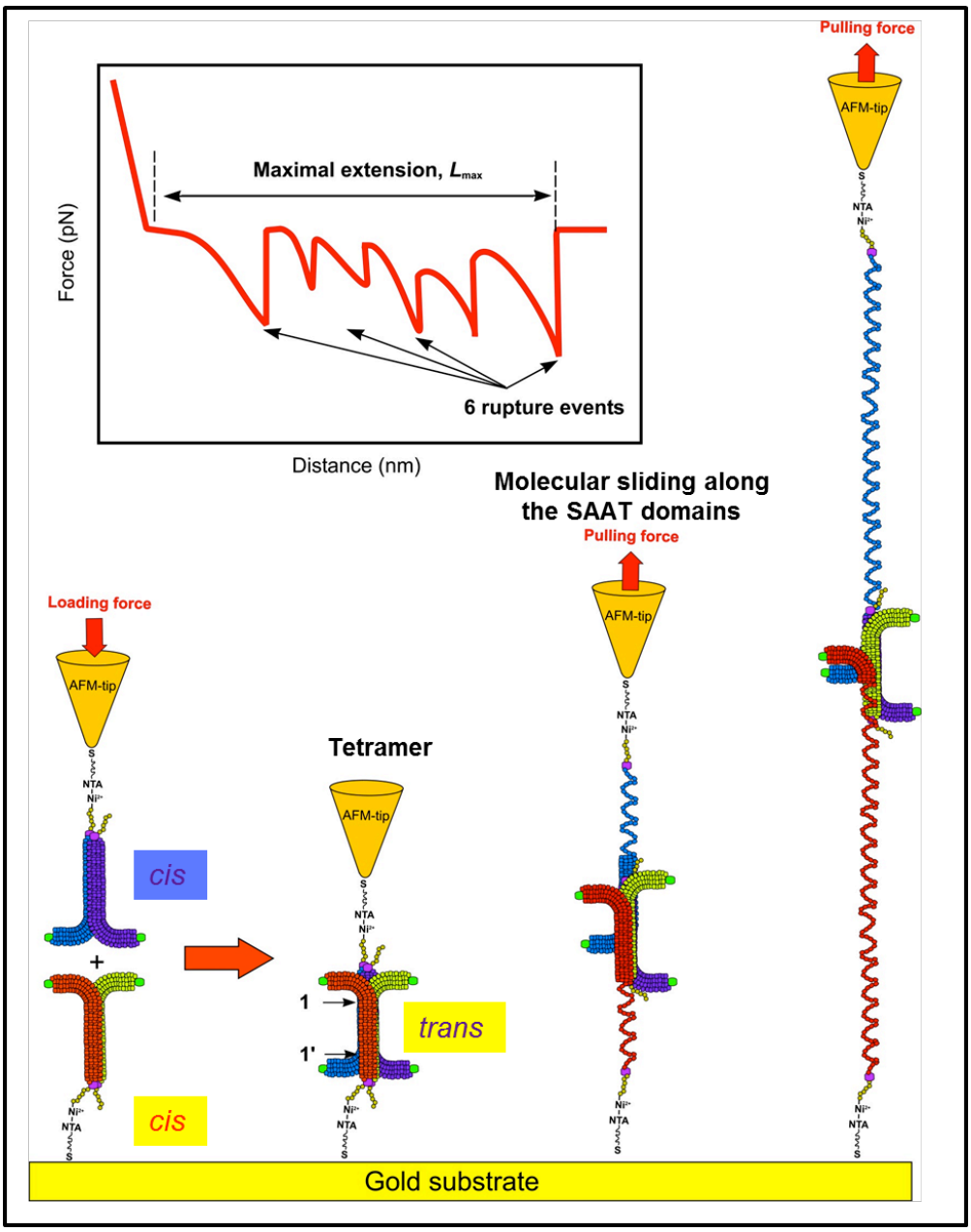

Figure 10. Schematic representation of the unfolding of Ag43α tetramer.

Schematic representation of the formation and possible unfolding of a tetramer of Ag43α formed by *trans*-interactions between two dimers in *cis*-configuration.